A general circulation model study of the dynamics of the upper ocean circulation of the South China Sea

Haijun Yang and Qinyu Liu
Physical Oceanography Laboratory, Ocean University of Qingdao, Qingdao, People's Republic of China

Zhengyu Liu
Department of Atmospheric and Oceanic Sciences, University of Wisconsin-Madison, Madison, Wisconsin, USA

Dongxiao Wang and Xiongbin Liu
South China Sea Institute of Oceanology, Chinese Academy of Sciences, Guangzhou, People's Republic of China

Received 5 August 2001; revised 29 November 2001; accepted 11 December 2001; published 30 July 2002.

[1] The temporal-spatial structure and the formation mechanisms of the South China Sea (SCS) circulation are studied using the Princeton Ocean Model (POM). The model well reproduces the observed sea surface height (SSH) annual cycle and some current system such as the SCS Western Boundary Current (SCSWBC) system and the Kuroshio Loop Current (KLC). Four sensitivity experiments are carried out to reveal the dynamic mechanisms of the SCS circulation. The results show that most of the seasonal variability of the SCS is controlled predominantly by wind forcing. The Kuroshio affects the mean SSH significantly but contribute little to the variability. The SCSWBC system consists of the SCS Warm Current (SCSWC) and the Vietnam Coastal Current (VCC). In winter the SCSWBC splits into two branches separated at $\sim$14°–18°N. The northern branch is the SCSWC flowing northward and the southern branch is the VCC flowing southward. In summer, however, the SCSWBC flows unidirectionally northward from the Karimata Strait to the Taiwan Strait. The temporal variation of the SCSWBC, especially the VCC, is determined by the wind forcing over the interior SCS. Buoyancy forcing can strengthen (weaken) the summer (winter) SCSWBC. The KLC is crucial to the SCS circulation north of 18°N. It ultimately determines the appearance of the SCSWC in winter. *INDEX TERMS:* 4255 Oceanography: General: Numerical modeling; 4512 Oceanography: Physical: Currents; 4532 Oceanography: Physical: General circulation; 4576 Oceanography: Physical: Western boundary currents; *KEYWORDS:* South China Sea circulation, South China Sea Western Boundary Current, South China Sea Warm Current, Vietnam Coastal Current, Kuroshio Loop Current

1. Introduction

[2] The South China Sea (SCS) is the largest marginal sea in the Southeast Asia with a total area of 3.5 million km^2 and an average depth of over 2000 m (Figure 1). It is connected with East China Sea, the Pacific Ocean, the Sulu Sea, the Java Sea, and the Indian Ocean through the Taiwan Strait, the Luzon Strait, the Palawan and Balabac Straits, the Gasper and Karimata Straits, and the Strait of Malacca, respectively. The Luzon Strait is most important to the SCS because it has a width of $\sim$300 km and a maximum depth of 2400 m. The climate of the SCS belongs to the Southeast Asia monsoon system [*Wyrtki*, 1961]. In winter the SCS is dominated by the northeasterly monsoon with an average wind speed of $\sim$9 m s^{-1}, while in summer, the wind direction completely reverses to southwesterlies with an average speed of 6 m s^{-1} (Figure 2). The wind forcing and topographic features determine that, first, the upper ocean circulation within SCS has a dramatic seasonal variability driven by the SCS monsoon wind [*Wyrtki*, 1961], and second, the northern SCS circulation would be significantly affected by the Kuroshio Current through the Luzon Strait.

[3] From observational evidence and results of ocean general circulation models (OGCM), it has been established that the basin-scale circulation in the SCS is cyclonic in winter and anticyclonic in summer [*Wyrtki*, 1961; *Xu et al.*, 1980; *Shaw and Chao*, 1994; *Metzger and Hurburt*, 1996; *Chu et al.*, 1999, hereinafter referred to as CHU; *Ho et al.*, 2000, hereinafter referred to as HCR; *Liu et al.*, 2001, hereinafter referred to as LYL]. The dynamics of the seasonal variability of the SCS circulation is closely related to the SCS monsoon. Recent observations of TOPEX/POSEIDON (T/P) (HCR; LYL) show that the SCS sea surface height (SSH) is low (high) in winter (summer), consistent with a (an) cyclonic (anticyclonic) circulation. It is very interesting to notice that the SCS SSH anomaly (SSHA) in winter and spring is exact out of phase with that in summer and fall. This

0148-0227/02/2001JC001084$09.00

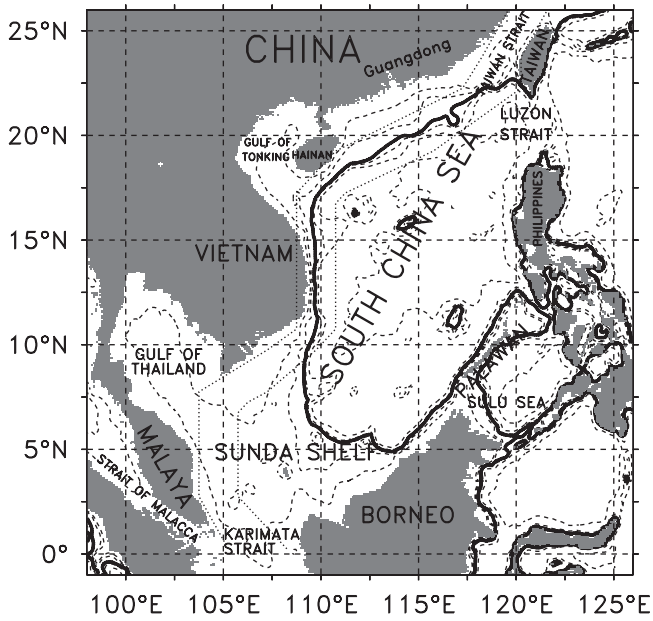

Figure 1. Bathymetry of the South China Sea (SCS). The 300-m isobath is indicated by heavy line. Dotted lines show the path of the SCS Western Boundary Current.

feature is mainly caused by the regional monsoon wind, which is also exact out of phase with each other in winter and summer (Figure 2; LYL).

[4] LYL studied the regional dynamics and established a simple and unified dynamic frame of the SCS seasonal variability based on two independent data sets (T/P altimetry data [*Chambers et al.*, 1997] and Levitus climatological hydrography [*Levitus and Bayer*, 1994a, 1994b]) as well as two theoretical models. Seasonal variability of the SCS circulation is interpreted in light of large-scale dynamics and Rossby waves. Because of smallness of the SCS ocean basin, the baroclinic Rossby wave with the wave speeds of 40 cm s^{-1} (for southern SCS) to 10 cm s^{-1} (for northern SCS) crosses the SCS (of ~1000 km) in 1 to 4 months. This short thermocline adjustment time implies that the upper ocean circulation is always in quasi-steady Sverdrup balance on the annual period. Therefore the SSH variability is mainly forced by the surface wind curl on the baroclinic Rossby wave. In addition, LYL also found that by analyzing the steric height anomaly (SHA) calculated from Levitus climatological data, the surface heat flux tends to enhance the wind-generated variability. The surface SHA (for upper 50 m), which reflects the expansion/contraction of the water column in the mixed layer in response to surface heat flux, accounts for 20% of the total SHA. Moreover, because the surface SHA has a similar pattern with the total SSH, the dynamic SSH (the total SSH minus the surface SHA), which reflects the effect of Ekman pumping forced by wind curl, also has a similar spatial distribution with the total SSH and accounts for 80% of the total SSH. This suggests that the seasonal cycle of the SCS is determined predominantly by the wind forcing over the SCS. The surface heat flux has a secondary effect on the seasonal variability of the SCS circulation.

[5] However, LYL focus on the interior ocean of the SCS. The oversmoothed T/P data and Levitus data as well as the simple models in LYL do not reflect some smaller scale features that eventually consist of indispensable components of the SCS circulation, such as the western boundary current [*Yang*, 2000] and the Kuroshio Loop Current (KLC) in the Luzon Strait [*Li and Wu*, 1989; *Metzger and Hurburt*, 1996; *Liu and Liu.*, 1996]. Naturally, this brings up the necessity of simulating the SCS circulation using a high-resolution OGCM. There have been lots of numerical studies on the SCS circulation, which cover almost every aspect of the SCS circulation [e.g., *Shaw and Chao*, 1994; *Chao et al.*, 1995; *Chao and Shaw*, 1996a, 1996b; *Metzger and Hurburt*, 1996; *Chu et al.*, 1999]. For example, more recently, CHU studied the seasonal ocean circulation and thermal structure in the SCS using the Princeton Ocean Model (POM) with a very high spatial resolution. The simulated general basin-scale structures of the SCS correspond with observations and other author's simulations very well. Furthermore, he conducted three sensitivity experiments and concluded that nonlinearity is important to the transport of baroclinic eddy features, transport from lateral boundaries is crucial to the

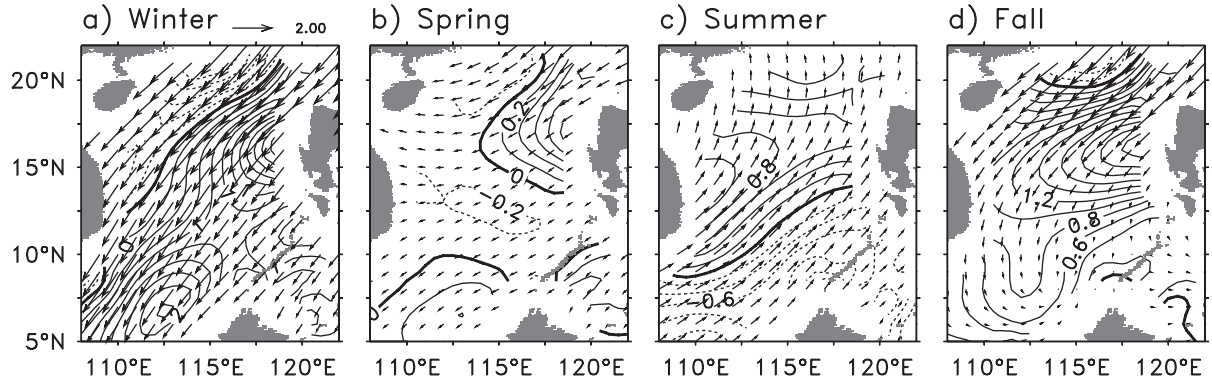

Figure 2. Seasonal mean Comprehensive Ocean-Atmosphere Data Set (COADS) wind stress τ/ρ_0 (vectors, 10^{-5} m^2 s^{-2}) and wind stress curl $curl(\tau/\rho_0)$ (CI = 0.2 × 10^{-10} m s^{-2}) for (a) winter (December–February), (b) spring (March–May), (c) summer (June–August), and (d) fall (September–November). Dashed lines indicate negative values.

summer circulation and thermal structure, with less effect on winter hydrology. In addition, he studied the western boundary current's seasonal variability and the variability of a mesoscale eddy generated in his model and obtained some interesting conclusions.

[6] In spite of relatively reasonable simulations by these authors, observations (for example, T/P altimetry and Levitus climatological data) require that the numerical simulation on the SCS circulation, even for the annual cycle climatology of the SCS circulation, still need to be greatly improved. For example, the SCS warm current (SCSWC), existing in the northern SCS in both winter and summer, found by several hydrological investigations by Chinese scientists and the International Corporation Plan [*Guan*, 1978, 1990, 1998], is hard to be identified in the mean circulation field of those simulations. The KLC in the Luzon Strait, supported by observations [*Wyrtki*, 1961; *Li and Wu*, 1989; *Shaw*, 1991; *Pu et al.*, 1992], is not very well simulated by previous works. In addition, the simulation of some coastal upwelling processes, e.g., the Luzon Cold Eddy (LCE), which can be identified clearly from Levitus data [*Shaw*, 1996; *Yang and Liu*, 1999] and T/P altimetry (HCR; LYL), and Vietnam coastal upwelling, which can be seen from T/P altimetry and National Oceanic and Atmospheric Administration (NOAA) Advanced Very High Resolution Radiometers (AVHRR) IR image (HCR), are far from satisfactory.

[7] These problems stimulate the studies in this paper. Here we will first describe the mean annual cycle of the SCS general circulation simulated in our model, along with the comparison to observations in order to convince people of the validity of the simulations, and then focus on discussing the seasonal variability and the formation mechanism of the SCSWBC, SCSWC as well as the effect of the KLC on the SCS. Four sensitivity experiments are conducted to individually explore the effects of the wind forcing, buoyancy forcing and boundary forcing on the SCS circulation. This paper is arranged as follow, section 2 is the description of the ocean model. Section 3 describes the mean SCS circulation from our control run and the detailed comparisons with observations. Section 4 focuses on formation mechanisms of the SCS current system. A summary and some discussions are presented in section 5. The SCS seasons in this paper are defined as, winter is December through February, spring is March through May, summer is June through August, and fall is September through November.

2. Model and Data

[8] The three-dimensional Princeton Ocean Model (POM) with realistic topography and a free surface [*Blumberg and Mellor*, 1987, hereinafter referred to as BM] is used. The bottom stress and surface wind forcing have the same form as that in BM and CHU, except that Comprehensive Ocean-Atmosphere Data Set (COADS) climatological wind stress is applied for all POM experiments in this paper.

[9] The model has a domain that includes almost the entire Pacific, ranging from 20°S to 45°N and from 98°E to 70°W. The model grids in Indian and Atlantic Ocean are treated as land and do not take part in calculation in model. So that the model ocean only includes the SCS, the Pacific Ocean as well as most part of the Japan Sea. Nonuniform horizontal resolution is used here to save computer time without sacrificing resolution within the SCS. In the SCS region (0°–30°N, 98°E–125°E), the grid interval is $0.5° \times 0.5°$ in both meridional and zonal directions. Outside of the SCS, from the SCS boundaries to model boundaries, the grid interval increases linearly from 0.5° to 2° in the meridional direction and to 5° in the zonal direction. The model has 15 vertical sigma levels so that the total model grid points are $116 \times 90 \times 15$. The minimum and maximum depth for the model are 10 and 4500 m, respectively.

[10] The reasons to apply the POM to the Pacific are, first, the mass transport through the SCS straits (especially the Luzon Strait) has a significant influence on the SCS circulation. In other words, the setting of lateral boundary conditions for the SCS is crucial to at least the northern SCS circulation, yet up-to-date observations of the mean annual cycle of mass transport through those straits are not available. Most previous simulations of the SCS used the value from Wyrtki [*Wyrtki*, 1961; *Shaw and Chao*, 1994; *Chao and Shaw*, 1996a, 1996b; CHU]. This might result in some inaccuracy in modeling the KLC in the Luzon Strait and the northern SCS circulation, as well as the SCSWC. This dilemma is avoided in this paper by setting the model domain much larger than the SCS itself. Second, the closed lateral boundary condition can be used for model region to exclude some error caused by boundary radiation or reflection rising from the numerical scheme of the boundary equation. The northern and southern boundaries can be solid because in the Pacific the wind curls at 20°S and 45°N are approximately equal to zero [*Hellerman and Rosenstein*, 1983], so that the meridional Sverdrup transport also approaches zero at these two latitudes. The mass exchange across these two latitudes should not significantly affect the SCS circulation on the annual time scale.

[11] The POM is initialized with the annual mean Levitus temperature and salinity [*Levitus and Bayer*, 1994a, 1994b]. The surface heat flux is calculated as a restoring toward the climatological annual cycle of SST with the restoring coefficient calculated from COADS data [*da Silva et al.*, 1994]; the surface salinity flux is calculated with the E-P (evaporation minus precipitation) climatology from COADS [*da Silva et al.*, 1994]. The model is run for 10 years for all experiments, of which the last 5 years of simulation are composed into a seasonal cycle. The POM has several particularly desirable features that are lacking in the simple LYL models: it has more complete dynamics, such as boundary currents, mesoscale eddies, bottom topography, and nonlinearity; it includes the surface steric response to heat flux forcing, which usually accounts for a large part of the annual cycle of SSH in the extratropics; and it also includes coastal upwelling processes, which may be important for small oceans such as the SCS. It is expected that the model simulation can not only match the dynamics of the seasonal variability studied in LYL, but also give more reasonable mean circulation climatology.

[12] One control run (EXP1) and four sensitivity experiments are carried out to address the individual effects of wind forcing, buoyancy forcing, open boundaries, and the

Table 1. Scheme of the Four Sensitivity Experiments

Experiments	Scheme
EXP2 (NO-HEAT)	no buoyancy forcing
EXP3 (NO-WIND)	no wind forcing
EXP4 (NO-KUROSHIO)	closing the Luzon Strait
EXP5 (NO-OPEN)	closing all straits

Kuroshio Current on the SCS circulation. They are designed as follows (Table 1):

[13] Altimeter observation from TOPEX/POSEIDON (T/P) mission [*Chambers et al.*, 1997] is used to provide comparison with modeling SSH. The T/P altimetry data spanning from 1992 to 1998 is composed into a seasonal climatology. It has been corrected for all media and instrument effects (ionosphere, wet and dry troposphere, and electromagnetic bias) and geophysical effects (tides and inverted barometer) [*Chambers et al.*, 1997]. We use a gridded/smoothed version ($1^\circ \times 1^\circ$ resolution) compiled by the Center for Space Research, University of Texas. The spatial filter used for the data is a rectangular Gaussian-squared filter spanning 1000 km in longitude and 450 km in latitude. The T/P data, with the nearest track 200 km away, may not capture small-scale features realistically, it should, however, be reasonably adequate for basin-scale features in the SCS.

3. SSH and SSH Anomaly

[14] Let's first briefly describe the mean annual cycle of the SSH and its seasonal variability (Figures 3a and 3b). The winter SSH (Figure 3a) in the whole basin is relatively low, with two low centers, located in the north ($14^\circ-18^\circ$N) and south ($4^\circ-12^\circ$N) respectively. The southern low center is weaker but larger in area than the northern one. In the Luzon Strait the SSH contours extend westward into the SCS and form an anticyclonic loop when going from south to north. The winter SSH pattern implies a basin scale cyclonic circulation, with two mesoscale cyclonic gyres in the south and north. In spring, the SSH of the whole basin increases and the basin-scale circulation reverses to an anticyclonic circulation. The SSH in summer is very similar to that in spring. The pattern of implied circulation is almost out of phase with that in winter. In fall the SSH is low again with a pattern similar to that in winter.

[15] The mean SSH pattern corresponds well with the dynamic height calculated from historical hydrological data [*Xu et al.*, 1980] as well as simulations by other authors [*Li and Zeng*, 1993; *Li et al.*, 1994]. Notice that a quite remarkable feature of the mean SSH is the anticyclonic bend of the SSH contours in the Luzon Strait throughout a year. This corresponds with the KLC [*Li et al.*, 1998; *Liu and Liu*, 1996]. Our model clearly exhibits the seasonal variations of the KLC: in winter and spring the KLC has less deformation, which implies a reduced dynamic effect of the Kuroshio Current on the SCS. It is worth noting that in summer and fall, the overwestward extension of the KLC eventually generates a closed, anticyclonic, mesoscale eddy, seen as a detached ring from the main axis of the Kuroshio Current [*Li et al.*, 1998], which dynamics has been elaborated by *Li et al.* [1998].

[16] The seasonal mean SSHA of the control run (Figure 3b) is very consistent with T/P altimetry (Figure 3c; also Plate 1 by HCR and Figure 3 by LYL) and the Levitus SHA (Figure 3d; also Figure 3 by LYL) as well as the simple models (Figure 5 by LYL). The winter pattern (Figure 3b) is dominated by a low (negative) SSHA centered along the Philippines with an amplitude of 8 cm, which is almost identical to that of T/P and Levitus. In spring a high (positive) SSHA is centered against the coast off Vietnam and tends to shift eastward and northward toward the Philippines during summer. The summer pattern is exactly out of phase with that in winter but has the same amplitude. In fall the reverse occurs to the SSHA, a low (negative) SSHA occupies the central SCS. Here we notice that the simulated high (low) SSHA in the central SCS in spring (fall) is much larger in area than observations. This difference may be due to the oversmoothed T/P data as well as the interpolation error of the T/P data.

[17] Not only the spatial pattern but also the temporal evolution and amplitude of the seasonal variability of the modeling SSH well correspond with the observations. Figure 4 shows the time evolution of the zonal-averaged POM SSHA, T/P SSHA, and Levitus SHA for different zonal bands. The phase and amplitude of the SSHAs are matched very well for most regions of the SCS. For the northern basin ($18^\circ-20^\circ$N, Figure 4a), the SSHAs reach a maximum (minimum) during October and November (February and March) with amplitudes of $\sim$5–6 cm. For the southern basin ($10^\circ-18^\circ$N, Figure 4b) the SSHAs reach a maximum (minimum) in July (February) with amplitudes of 4–5 cm. The correlation coefficients of the simulation and the observations are over 0.6 for most of basin, and the ratio of standard deviations for the SSHAs are close to 1.0 (figure not shown).

[18] All above comparisons convince us of the validity of the modeling basin-scale circulation. This is further confirmed by the following sensitivity experiments (EXP2-5), which give the similar conclusions with those in the LYL analyses. EXP2 (Figure 5a) gives the results for only wind forcing, which explicitly exhibits the dynamic SSHA defined as in the works of LYL and *Gill and Niiler* [1973], and caused by Ekman pumping forcing on the density field in the thermocline. The dynamic SSHA can also be approximated from EXP1 (control run) by subtracting the surface steric height from the total SSH [*Gill and Niiler*, 1973]. EXP3 (Figure 5b) explicitly demonstrates the surface steric height (that is, the surface SSHA) reflecting the expansion/contraction of the water column in the mixed layer in response to surface heat flux and salinity flux (E-P) forcing. First of all, the spatial patterns of the dynamic SSHA in Figure 5a are almost identical to those in Figure 3b, while the patterns of the surface SSHA in Figure 5b more or less align with latitudes. Second, the amplitudes of the dynamic SSHA are slightly smaller than the total SSHA (Figure 3b), with the ratio of area averaged SSHA of EXP2 and EXP1 of $\sim$0.8. However, the amplitudes of the surface SSHA are much smaller than the total, with the ratio of no more than 0.2. These two experiments clarify that the Ekman pumping forcing contributes most of the variability of the SCS SSH, while the surface buoyancy flux donates little to the SCS basin-scale circulation. Notice that since the surface SSHAs (Figure 5b), especially those south of 14°N,

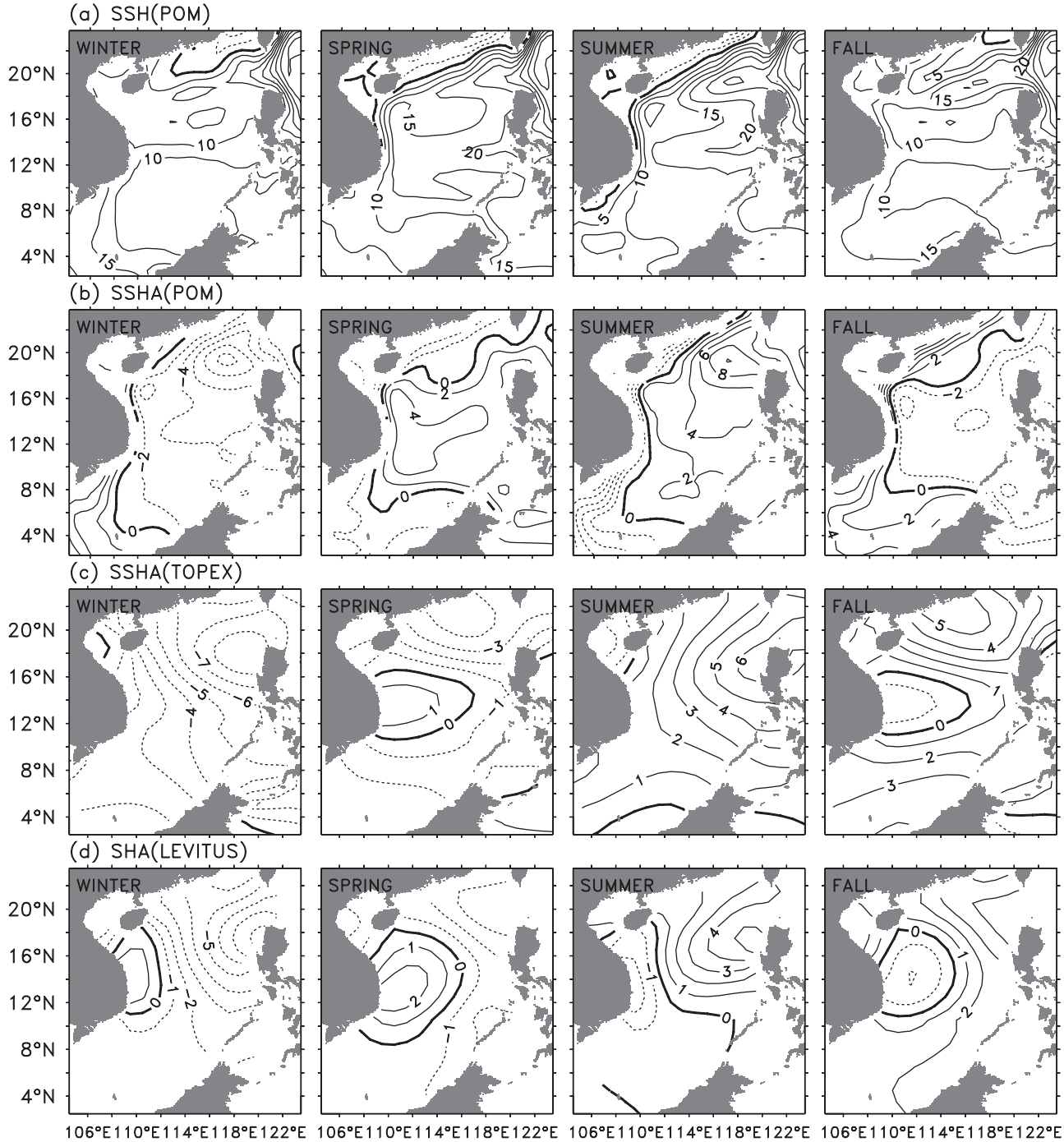

Figure 3. Seasonal mean sea surface height (SSH) and SSH anomaly (SSHA) from model and observations: (a) the seasonal mean SSH from control run (CI = 5 cm), (b) the SSHA from control run (CI = 2 cm), (c) the SSHA from TOPEX/POSEIDON (T/P) altimetry (CI = 1 cm), and (d) the Steric Height Anomaly (SHA) calculated from Levitus hydrological data (CI = 1 cm).

have spatial patterns nearly parallel to the latitudes and are different dramatically from the total SSHA (Figure 3b), therefore, the surface buoyancy flux south of 14°N does not contribute directly to the pressure gradient, in turn, the upper geostrophic flow. The SSHAs north of 14°N show somewhat similar to the total, implying a relatively important contribution to the upper ocean circulation. These analyses are slightly different from LYL's conclusions, in which they overestimated the contribution of the buoyancy flux to the basin-scale circulation, especially to the southern SCS circulation. This might be due to the uniform mixed layer depth assumed in their calculation of the surface steric height. Finally, the experiments with closed boundaries (Figures 5c and 5d) show similar patterns and amplitudes of the SSHA with little difference from the total SSHA (Figure 3b), which appear to emphasize that the regional

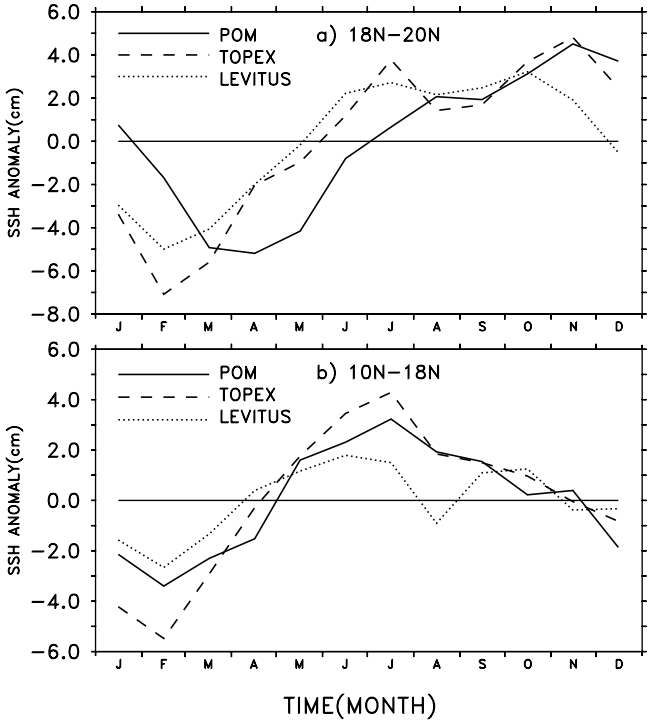

Figure 4. Temporal evolution of the zonal averaged (108°–120°E) SSHA for different zonal bands: (a) 18°–20°N and (b) 10°–18°N. Solid lines are for Princeton Ocean Model (POM) control run, dashed lines for T/P altimetry, and dotted lines for Levitus SHA.

dynamic forcing dominates the seasonal variability of the SCS circulation.

4. Upper Ocean Current

[19] The vertical thermal structure of the SCS has a strong thermocline, which can therefore be approximated by a 1.5-layer fluid (LYL). The mean stratification in the SCS gives the active upper layer with a depth of ~300 m. The smallness of the SCS basin determines that the adjustment time of the SCS thermocline by planetary wave is ~1 to 4 months (LYL). This is fast enough and, ultimately, results in the strongly baroclinic SCS circulation, in other words, the concentrated transport only in the upper ocean, under an annual cycle forcing (LYL). Therefore the SCS circulation reduces to the upper-ocean baroclinic Sverdrup balance. Consequently, in the following content, we only analyze the upper ocean current averaged from surface to 300-m depth.

[20] In general, the seasonal mean upper ocean current (Figure 6) is well simulated when compared to observational studies [*Wyrtki*, 1961; *Guan*, 1978; *Guo et al.*, 1985] and other simulations [*Shaw and Chao*, 1994; CHU]. Between 14° and 18°N, a remarkable cyclonic gyre exists for the whole year and hardly changes with time. In the deep-sea region of 12°–14°N an anticyclonic gyre persists regardless of season. Between 6° and 12°N, a cyclonic gyre exists in winter and fall and the opposite occurs in summer and spring. Here we pay more attention on the following current systems:

4.1. SCS Western Boundary Current System

[21] The SCSWBC system consists of the Vietnam Coastal Current (VCC) south of 18°N and the SCSWC between 18° and 23°N (Figure 6). It exists for the whole year and extends from the Karimata Strait to the Taiwan Strait [*Wyrtki*, 1961], in company with high variabilities of direction and strength. The SCSWBC in the SCS is the analog to the Kuroshio Current of the North Pacific or the Gulf Stream of the North Atlantic, which are mainly modulated by the forcing over the interior ocean. However, because of the smallness of the SCS basin, the SCSWBC does differ from the Kuroshio Current and Gulf Stream by its distinct seasonal variability.

4.1.1. Vietnam Coastal Current (VCC)

[22] As the southern portion of the SCSWBC, the VCC flows southward in winter and fall (Figures 6a and 6d). It splits into two branches over the Sunda Shelf: one branch turns to eastward and finally flows northeastward along the north coast of the Borneo Island; the other branch keeps flowing southward and eventually flows out of the SCS through the Karimata Strait. In spring and summer (Figures 6b and 6c) the VCC completely reverses to flow northward. It flows along the coast of Vietnam and the east of Hainan Island, and finally merges into the SCSWC.

[23] The existence for the VCC can be confirmed by Argos-tracked Buoys. We get the Buoy drifters from Marine Environmental Data Services (MEDS) in Canada (http://www.meds-sdmm.dfo-mpo.gc.ca/meds/Databases). The drifters selected in this paper were released between 1993 and 1996 and moving within the SCS region. The drifter system consists of three parts: a surface float with a transmitter, a subsurface float, and a drogue with a height of 6.44 m and a diameter of 92 cm [HCR]. After being released into the ocean, the system remained vertical to the ocean surface, and the depth of the center of drogue was ~15 m. Therefore the tracks of drifters represented the ocean current in the surface and subsurface layers. During the experiment the Argos Company was in charge of tracking the drifters and provided the data [*HCR*]. Table 2 lists the selected drifters' information that include the initially releasing date, latitude and longitude, and the finally recorded date, latitude, and longitude. Except drifter 22520, whose tracking period was from 23 June to 29August 1994, representing summer current, the other drifters represent approximately winter surface currents.

[24] One can see from Figure 7a that, the drifter 22801 released at 15.767°N and 109.625°E on 11 December 1993, moved all the way southward along the coast of Vietnam, and reached the Karimata Strait at 1.229°N and 104.567°E on 28 February 1994. The drifters 22513, 22515, and 22516 showed the same movement during the winter of 1995. The trajectories of these four drifters provided robust evidence that there does exist southward flowing VCC in winter, which is well simulated in our model (Figures 6a and 6d). It is worth to note that the drifter 22513 released on 21 September 1995, first moved southeastward, reaching its south most point at 12.775°N and 113.154°E on 26 September 1995, and then moved cyclonically northward, reaching its north most point at 15.055°N and 111.503°E on 9 October 1995, and finally joined the VCC around 20 October 1995. The cyclonic movement of drifter 22513

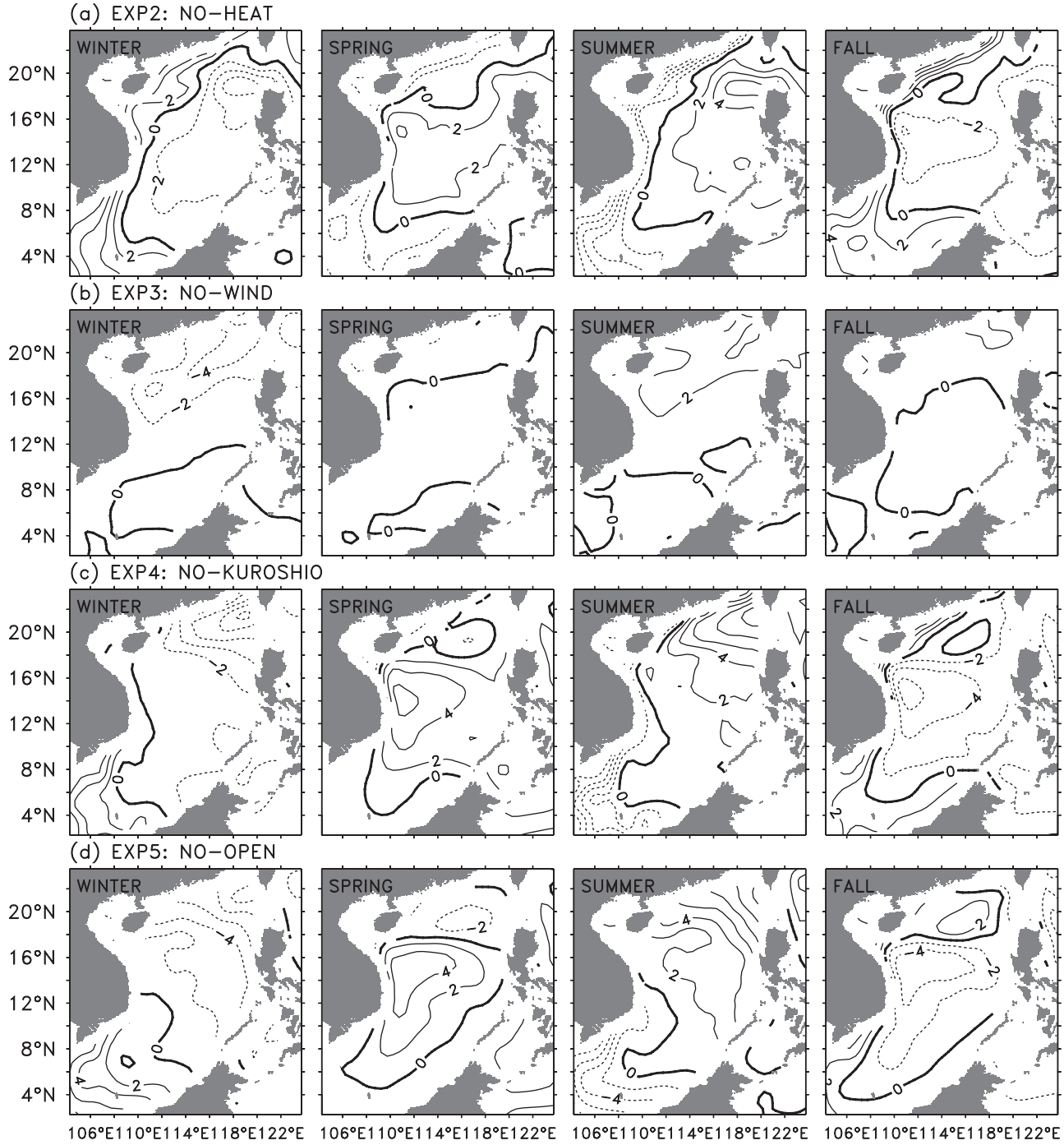

Figure 5. Seasonal mean SSH anomaly for sensitivity experiments (CI = 2 cm): (a) EXP2, (b) EXP3, (c) EXP4, and (d) EXP5.

from 21 September to 9 October 1995 implied a cyclonic circulation between 13° and 16°N near the coast of Vietnam, which is surprisingly reproduced in our model (Figure 6d).

[25] The drifter 22802 (Figure 7b), released at 13.595°N and 112.622°E on 22 December 1993, seemed to be first advected by surface Ekman flow whose direction is perpendicular to the winter southwestward monsoon, and then joined the VCC once it reached the western boundary. The movement of drifter 22804 (Figure 7b) was similar to those of drifters 22801, 22513, 22515, and 22516. However, there was a distinct difference between 22804 and other drifters: drifter 22804 turned to move northward after it reached its south most location at 7.76°N and 106.777°E on 6 March 1994 and maybe eventually hit the south coast of Vietnam at the end of this record. The trajectory of 22804 might provide direct evidence that the monsoon driven VCC changes its direction in spring from southward to northward because of the seasonal transition of the SCS monsoon system. However, one must keep in mind that there is also possible that the trajectories of drifters be distorted by

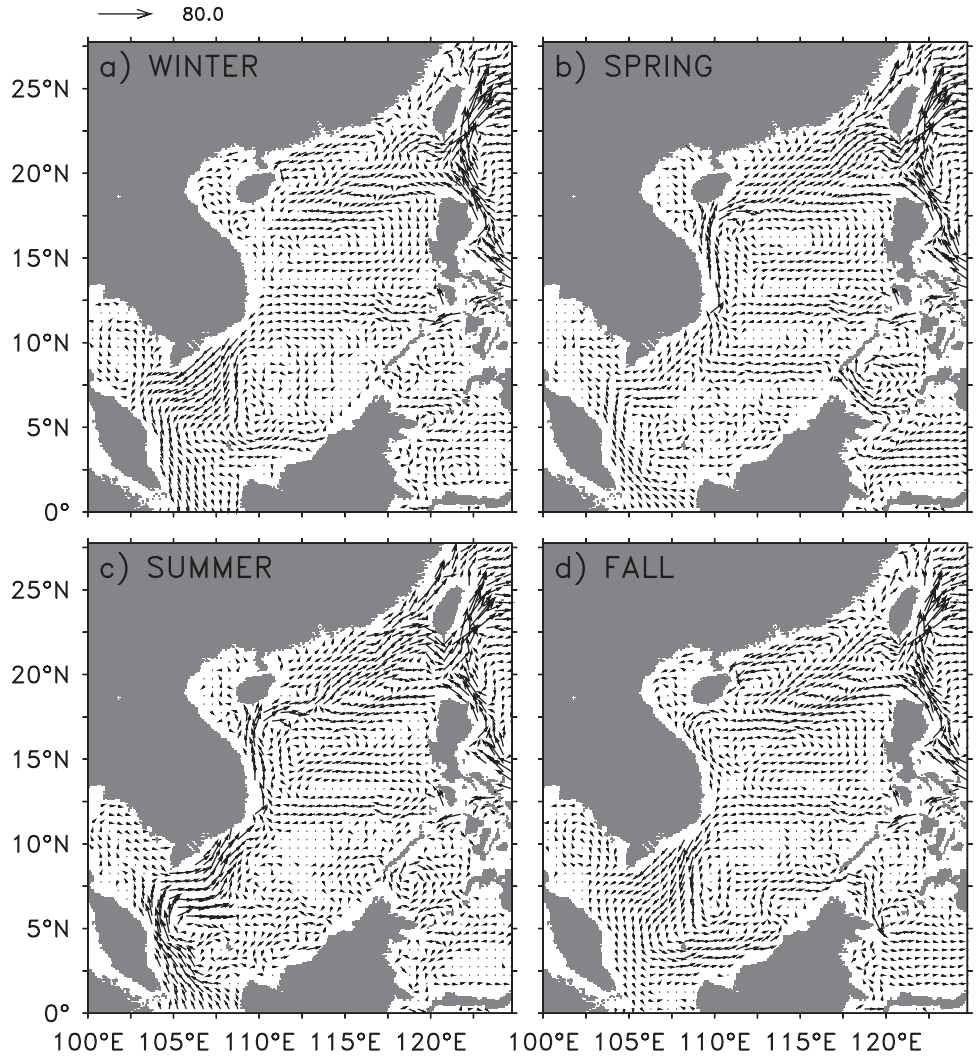

Figure 6. Seasonal mean upper ocean circulation averaged from surface to 300-m depth for control run: (a) winter, (b) spring, (c) summer, and (d) fall. The reference vector scale is 80 cm s^{-1}.

fishing boat. Therefore more observation evidences are needed to verify the VCC transition as simulated in our model (Figure 6).

[26] The dynamic mechanism of controlling the seasonal variation of the VCC can be understood by the classical Sverdrup circulation theory. The Sverdrup transport in the interior SCS is northward (southward) in winter (summer) because of cyclonic (anticyclonic) wind curl in winter (summer), which determines that the western boundary returning flow is southward (northward) in winter (summer). Moreover, because of the relatively short adjustment time of the SCS upper circulation, the VCC has a rigid annual cycle in response to annual wind forcing. We will return to this point later with more sensitivity experiments.

4.1.2. SCS Warm Current (SCSWC)

[27] The northern branch of the SCSWBC, that is, the SCSWC, represents a strong perpetual northeastward current nearly along the 300-m isobathic contour in the northern

Table 2. Drifter ID, Initially Releasing Date and Locations, Finally Recorded Date and Locations for Argos-Tracked Buoys

Drifter ID	Initial			Final		
	Date	Latitude, °N	Longitude, °E	Date	Latitude, °N	Longitude, °E
22801	11 Dec. 1993	15.767	109.625	28 Feb. 1994	1.229	104.567
22802	22 Dec. 1993	13.595	112.622	22 April 1994	15.375	109.099
22804	5 Jan. 1994	15.023	112.790	5 May 1994	10.402	107.220
22513	21 Sept. 1995	14.448	111.995	21 Dec. 1995	−0.163	108.708
22515	16 Nov. 1995	14.920	112.152	13 Jan. 1996	1.053	105.158
22516	16 Nov. 1995	13.037	111.080	5 Jan. 1996	−1.895	106.289
22520	23 June 1994	16.086	112.739	29 Aug. 1994	21.898	116.484

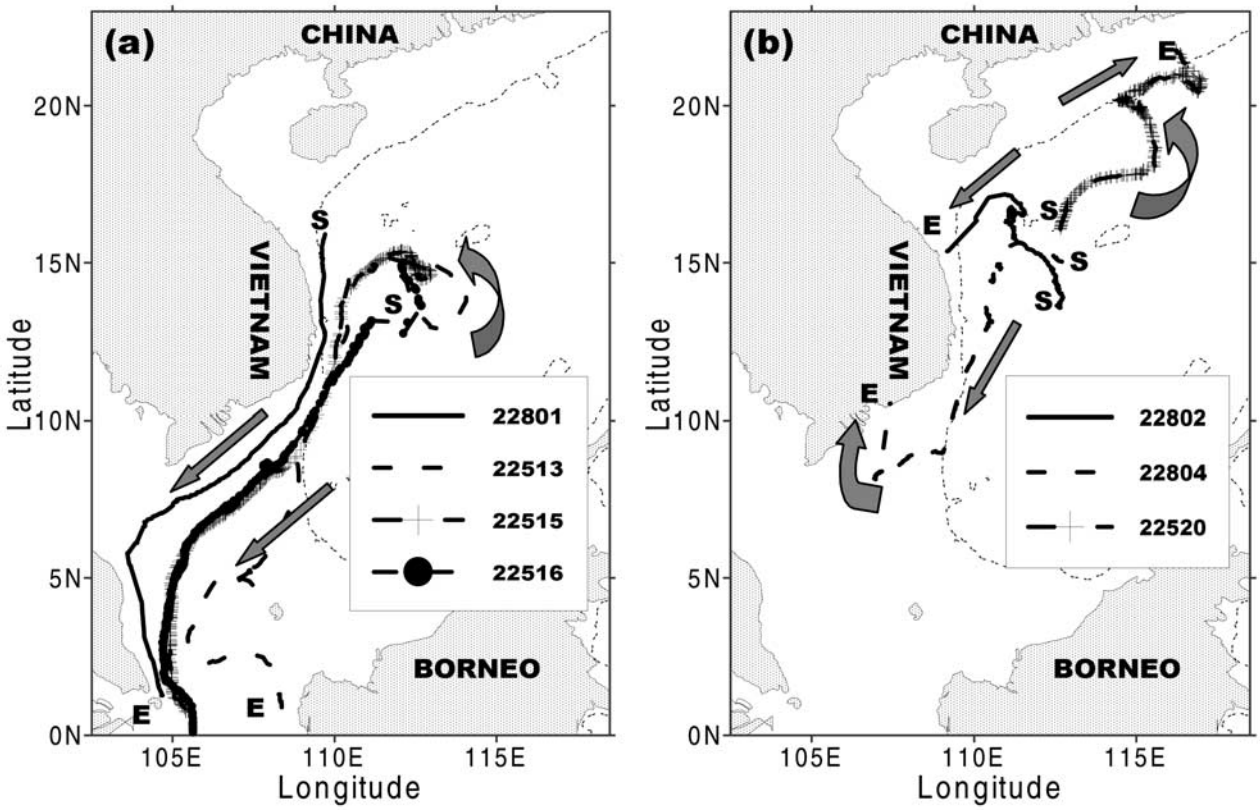

Figure 7. Trajectories of Argos-tracked drifters released in the SCS during 1993–1996. The "S" means starting points, and "E" means ending points. The solid arrows demonstrate the movement directions of drifters. The dashed line represents the 300-m isobathic contour of the SCS. (a) Drifters with ID 22801 (solid line), 22513 (dashed line), 22515 (dashed and cross line), and 22516 (dashed and dotted line). (b) Drifters with ID 22802 (solid line), 22804 (dashed line), and 22520 (dashed and cross line).

SCS, which has been observed by several oceanographic investigations [*Guan*, 1978; *Guo et al.*, 1985]. Figures 8a and 8b show two temperature sections observed during 23–24 February 1967 (hereafter, Section 1) and 1–14 January 1968 (Section 2), respectively. Section 1 was conducted by Japan Meteorology Agency "Ryofu Maru." It located off Shanwei-Jieshi bay and extended southeastward to 120°E, with the total span of more than 280 nautical miles [*Guan*, 1978]. The Section 2 was conducted by Hong Kong Fishery Institute "Cape St. Mary." This section located off Shantou coast and had a span of 120 nautical miles [*Guan*, 1978]. Figures 8c and 8d are the corresponding geostrophic velocities calculated from the observed temperature and salinity of Sections 1 and 2, where the numbers represent the magnitude of velocity, the positive (negative) values mean that the flow is northeastward (southwestward) with the direction being vertical to the sections' alignment. The locations of these two sections are plotted at the lower left corner of Figure 8a. It is worth to point out that the temperature structures (Figures 8a and 8b) of these two sections do favor a northeastward SCSWC in winter. The SCSWC is very strong from surface to 200-m depth (Figures 8c and 8d). Its velocity is more than 100 cm s^{-1} in above 100-m depth on Section 2 (Figure 8d). It looks weaker on Section 1 but still exceeds 30 cm/s in above 200-m depth (Figure 8c). The horizontal width of the SCSWC is beyond 60 nautical miles (~110 km) on Section 2 and even reaches 300 km on Section 1. It is undoubted that the SCSWC is the most important current in the northern SCS. The summer SCSWC is confirmed somewhat by the Argos-tracked Buoy. In Figure 7b the drifter 22520 that was released at 16.086°N and 112.739°E on 23 June 1994 moved northeastward first and then turned to nearly northward on 11 July. It moved northeastward again along 300 m isobathic contour during the entire August. Its trajectory in August clearly manifested the summer SCSWC.

[28] The simulated SCSWC (Figure 6) is quite consistent with those observations in both its velocity and horizontal scale. Model also reveals that the SCSWC is stronger and wider in summer (Figure 6c) than in winter (Figure 6a). The stronger SCSWC in summer is actually due to the coalescence with the Guangdong Coastal Current (GCC), which is also northeastward in summer. We will discuss GCC in section 4.2.

[29] One must notice that the SCSWC in the surface layer is also northeastward despite the surface southwestward winter monsoon (Figure 8). This suggests that SCSWC may not be driven by local wind. The SCSWC can be also understood by Sverdrup theory and western boundary current dynamics, in which the Rossby wave plays a critical role to maintain this current. As the western boundary

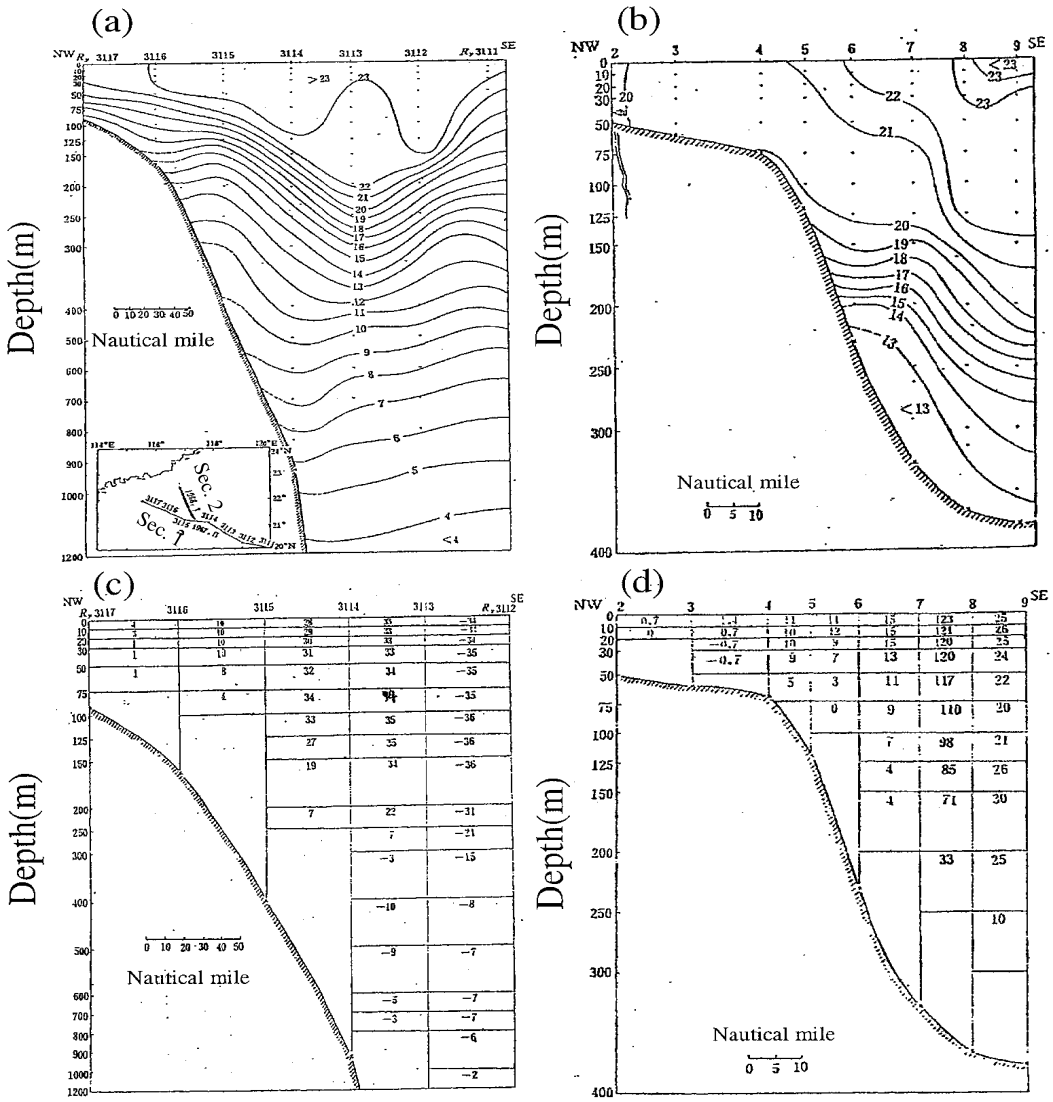

Figure 8. Depth section of temperature corresponding to two field investigations during February 1967 (Section 1) and January 1968 (Section 2), respectively: (a, c) Section 1 and (b, d) Section 2. The locations of two sections are plotted at the lower left corner of Figure 8a). The labels of horizontal axis in Figures 8a–8d specify the investigation station. The numbers in Figures 8c and 8d represent the magnitudes of geostrophic velocity (cm s^{-1}). Positive (negative) values in Figures 8c and 8d mean northeastward (southwestward) with the direction being vertical to the sections' alignment. These fours figures are scanned from *Guan* [1978].

current in the northern SCS, the SCSWC reflects the trapped short Rossby wave resulted from the interior long Rossby wave excited either in the interior SCS by wind forcing, or in the Luzon Strait by the Kuroshio Current. In winter and fall, because of the anticyclonic wind curl over the northern SCS (Figures 2a and 2d) as well as the anticyclonic loop current in the Luzon Strait caused by the Kuroshio Current, the SCSWC flows northeastward despite the local southwestward monsoon wind. In summer and spring the SCSWC seems to be more related to the northward VCC, that is, the anticyclonic wind curl over the southern SCS. We will examine SCSWC later through sensitivity experiments.

[30] It is worth noticing that there is a southwestward current on the southeast side of the SCSWC for the whole year (Figure 6). This current was first discovered by the comprehensive investigation of the northeastern SCS during 1967 [*Guan*, 1978; *Qiu et al.*, 1984; *Guo et al.*, 1985]. The speed, the horizontal width and vertical extension, as well as the mass transport, of this current are quite considerable. The observed temperature structure on Section 1 (Figure 8a), in which the temperature contours bend upward from station 3313 to station 3311, does imply a southwestward geostrophic current with the speed comparable to that of the SCSWC (Figure 8c). *Qiu et al.* [1984] and *Guo et al.* [1985] thought that this flow should

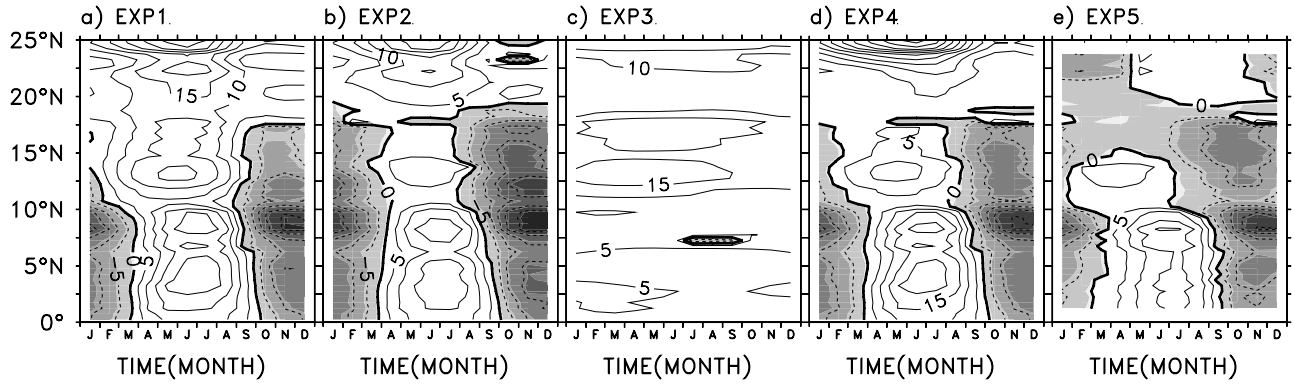

Figure 9. Latitude-time plot of the upper ocean SCSWBC ($(u^2 + v^2)^{1/2} * v/|v|$) averaged from surface to 300-m depth along the western boundary path (dotted line shown in Figure 1), CI = 5 cm s^{-1}: (a) EXP1, (b) EXP2, (c) EXP3, (d) EXP4, and (e) EXP5.

be seen as a branch of the Kuroshio Current in the SCS. They implied that the water from the Kuroshio Current could be transported far westward into the northern SCS and even reach the coast of Vietnam. However, there has no enough evidence yet to support their point. Our simulations show that it actually is the north frank of the northern SCS cyclonic gyre. This is consistent with the analyses of other researchers [*Liu and Su*, 1992; *Cai and Su*, 1995].

[31] Let's further explore the temporal and spatial variability of the SCSWBC through sensitivity experiments. We plot the time-latitude section of the upper ocean current $(u^2 + v^2)^{1/2} * v/|v|$ along the path of the SCSWBC (between the dotted line in Figure 1) for each experiment (Figure 9), where u and v are zonal and meridional component of SCSWBC, respectively. Figure 9 shows both the magnitude $(u^2 + v^2)^{1/2}$ and the direction $v/|v|$ of the SCSWBC. For control run (EXP1, Figure 9a), the SCSWBC in summertime (April to September) is unidirectionally northward from the Karimata Strait to Taiwan Strait with the maximum speed of 20 cm s^{-1} located at ~5°N, 13°N and 23°N, respectively, during June and July. In wintertime (October to March) it splits into two branches at the latitudes between 14° and 18°N. The SCSWC flows northward against the winter monsoon, and has a maximum speed of 20 cm s^{-1} in the Taiwan Strait in February. The VCC flows southward to the Karimata Strait and has a maximum speed of 25 cm s^{-1} at 10°N in November.

[32] EXP2 (Figure 9b) shows that the SCSWBC south of 10°N changes slightly when compared to that of EXP1. The wintertime (summertime) southward (northward) speed becomes a little bit larger (smaller). However, the southward (northward) SCSWBC between 10° and 18°N in winter (summer) changes sharply, which is ~3 times larger (smaller) than that of EXP1. The SCSWBC north of 18°N is also weaker than that of EXP1 although the direction does not change. EXP2 implies that the surface buoyancy flux would be in favor of driving a northward WBC for all seasons.

[33] EXP3 (Figure 9c) indicates that the SCSWBC does not change much throughout a year when the wind forcing is excluded for this experiment. It flows unidirectionally from south to north with a speed of 5 cm s^{-1} south of 10°N and 10–15 cm s^{-1} between 10° and 18°N. Actually, the EXP3 reflects the results of only buoyancy forcing because the Kuroshio Current in this case is negligible owing to no wind-forced Sverdrup flow in the interior Pacific Ocean. Therefore EXP3 not only shows that the buoyancy forcing can generate a northward SCSWBC throughout the year, that is, the basin-scale anticyclonic circulation, but also implies, from the contrary side, that the seasonal variability of the SCSWBC is controlled by wind forcing and the Kuroshio Current.

[34] In order to make clear the contribution of the Kuroshio Current to the SCSWBC, we close the Luzon Strait to exclude its effect. EXP4 (Figure 9d) reveals that the WBC south of 10°N does not change at all, and the WBC between 14° and 18°N reduces slightly. However, the SCSWC between 18° and 22°N reduces significantly and even disappears in winter. This suggests that the Kuroshio Current has notable effect on the circulation north of 14°N, enforcing the SCSWC in winter. Since in winter the SCSWC has little connection with the VCC, EXP4 indicates that it is the Kuroshio, not the monsoon wind, determines the appearance of the winter SCSWC.

[35] When closing all straits, we find from EXP5 (Figure 9e) that the SCSWBC hardly changes in the south, implying that the VCC in winter (summer) does not flow to (from) the Karimata Strait but rather the eastern basin. In other words, the water mass exchange through the Karimata Strait is not large enough to affect the SCSWBC and, in turn, the SCS circulation. However, the northern WBC changes dramatically. There is almost no SCSWC throughout the whole year. This is due to the combined effect of the wind forcing and buoyancy forcing. Taking into account EXP3, it implies that the wind forcing (local or remote) over the SCS could not force a northward SCSWC but does drive a southward WBC north of 14°N.

[36] Now it comes to the following conclusions based on the above analyses. First, the temporal variation of the SCSWBC, especially the VCC, is determined by the wind forcing. Second, the buoyancy forcing helps to drive a northward WBC. Third, the Kuroshio Current is crucial to the SCSWC. It controls the SCSWC in winter. Fourth, the mass transport through the Karimata Strait has little effect on the SCS circulation, and the VCC mainly comes from (flows to) the eastern basin.

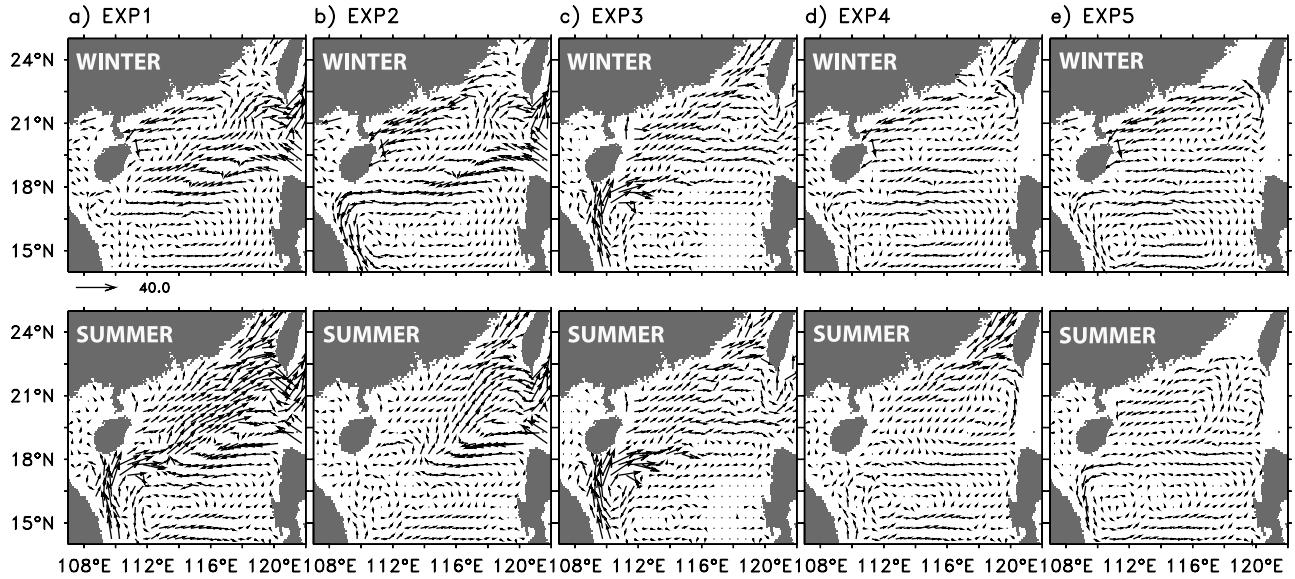

Figure 10. Upper ocean circulation averaged from surface to 300-m depth for the northern SCS: (a) EXP1, (b) EXP2, (c) EXP3, (d) EXP4, and (e) EXP5. The top panel is for winter and the bottom for summer. The reference vector scale is 40 cm s^{-1}.

[37] Let's continue the discussion of water sources for the SCSWC. We have known that the SCSWBC splits at about 18°N in winter, but flows continuously from south to north in summer (Figure 9a). This implies that the winter SCSWC does not include water south of 18°N, while the summer SCSWC is the extension of the southern WBC. From EXP2, 3, 4, we have found the winter wind forcing and the buoyancy forcing exert similar intensity but opposite effects on the northern SCS circulation. Therefore the Kuroshio Current is the only reason to produce the SCSWC in winter, furthermore, the winter SCSWC water can only come from the southwestward current [*Guo et al.*, 1985] on the east side. This southwestward current is very strong (Figures 10a and 10b) (weak, Figures 10d and 10e) with (without) the Kuroshio Current, substantially modulating the SCSWC in winter. It shows clearly that the winter southwestward current along 18°N in EXP1 and EXP2 (Figures 10a and 10b) is much stronger than that in EXP4 and EXP5 (Figures 10d and 10e), and actually disappears in EXP3 (Figure 10c). There are two ways of affecting the southwestward current by the Kuroshio Current, one is the direct water supply from the Kuroshio Current, and the other is dynamic intensification of the northern SCS cyclonic circulation by the KLC, by means of generating positive potential vorticity [*Liu et al.*, 2001], in the northwest region off the Luzon Island. The southwestward current can be seen as the north branch of the cyclonic circulation. In summer the SCSWC gets wider because of the mergence with the GCC. Figure 10 (lower panel) shows that part of the summer SCSWC water comes from the southern WBC. The Kuroshio remains to be important to SCSWC because the SCSWC is reduced significantly without the Kuroshio Current (the lower panel of Figure 10d).

4.2. Guangdong Coastal Current

[38] We have mentioned Guangdong Coastal Current (GCC) in the previous section. It locates off the coast of Guangdong Province, in the open sea north of 16°N. In winter the GCC flows southwestward reaching east of Hainan Island (Figure 6a); in spring and continuing through summer the GCC reverses to flow northeastward (Figures 6b and 6c); in fall the GCC turns to be southwestward again (Figure 6d). The GCC is strongly supported by several field investigations by Chinese scientists [*Rong*, 1994; *Hu and Liu*, 1992], for examples, the comprehensive investigations on the China Sea from September 1958 to May 1960 by China National Ocean Administration [*Guan*, 1978] and the investigation on the Southern Taiwan Strait during December 1987 by Xiamen University [*Hu and Liu*, 1992]. The winter GCC is measured at ~0.2–0.7 knot (10–40 cm s^{-1}) [*Rong*, 1994]. The simulated GCC reproduces the observations very well for both direction and speed. Furthermore, the model reveals that the GCC does not come from the Taiwan Strait even during the period of winter monsoon (Figure 6a).

[39] The GCC seems to be the manifestation of the trapped coastal Kelvin wave that is primarily modulated by the local wind forcing. The winter southwestward monsoon piles up water along the Guangdong coast and build a pressure field with the gradient southeastward, which is nearly perpendicular to the wind direction. Therefore, the coastal current has to be southwestward in corresponding with this kind of pressure field by the coastal Kelvin wave. In summer the opposite occurs. The northeastward monsoon establishes northwestward pressure gradient along the coast and forces northeastward coastal current. One can see that in Figure 3a, the SSH distributions over the continental shelf of the northern SCS are exactly associated with the direction of the GCC. Because of the seasonal variation of the local monsoon wind, the GCC also has a remarkable seasonal variation in response to the fast adjustment of the coastal Kelvin wave.

4.3. Current in the Taiwan Strait

[40] Figure 6 shows that the mass transport in the Taiwan Strait is northward throughout a year. The northward trans-

port in winter and fall is slightly weaker than that in summer and spring. Since there are relatively plenty of observations, it has been reached a coincidence that [*Rong*, 1994; *Hu and Liu*, 1992] the current in the Taiwan Strait flows northward during summer monsoon; during the winter monsoon, the strait is dominated by northward flow except along the coastal region off Guangdong Province [*Hu and Liu*, 1992]. It is possible that a southwestward flow temporarily appears in only the surface layer forced by continuously strong northeast monsoon. In any case the current below the surface layer always flows northward. In fact, the current in the Taiwan Strait is not decided by local forcing but by remote effect. The northward SCSWC should have great contribution to the northward mass transport in the Taiwan Strait throughout a year.

4.4. Kuroshio Loop Current

[41] It is illustrated clearly (Figure 6) that the KLC goes anticyclonically from south to north in the Luzon Strait [*Pu et al.*, 1992; *Liu and Liu*, 1996]. As a portion of western boundary current in the Pacific Ocean, the variability of KLC is actually dominated by the dynamics of the Pacific Ocean [*Metzger and Hurburt*, 1996]. Since the northern SCS circulation is strongly modulated by the KLC, consequently, the KLC plays a bridge for the interaction between the Pacific Ocean and the SCS. The simulations indicate that water south of 20°N in the Luzon Strait is transported westward into the SCS, and eastward into the Pacific at the other latitudes. This pattern is nearly constant with time, which is consistent with observations [*Guan*, 1990; *Wyrtki*, 1961]. We do not intend to discuss the KLC in detail here since our focus is on the SCS circulation.

5. Conclusions and Discussions

[42] The Princeton Ocean Model (POM) is used to study the seasonal mean SCS circulation and its formation mechanisms. It well reproduces the observed SSH annual cycle, explicitly resolving coastal current such as the VCC, the GCC, and the SCSWC. Sensitivity experiments show that the wind forcing dominates the seasonal variability of the SCS SSH, while the buoyancy forcing is of minor importance. Model also indicates that the Kuroshio Current affects the SCS circulation by creating a loop current that exists throughout the year.

[43] We proposed the concept of the SCSWBC system in this paper. The SCSWBC system consists of the SCSWC in the northern SCS and the VCC along the coastal of Vietnam. The POM simulates the SCSWBC very well. Both the direction and intensity of the SCSWBC change remarkably with time. The summer SCSWBC flows northward from the Karimata Strait to Taiwan Strait, while the winter SCSWBC splits into two branches between the latitudes of 14°–18°N. The north branch is the SCSWC and the south branch is the VCC. Sensitivity experiments indicate that the temporal variation of the SCSWBC is determined by wind forcing over the interior SCS. Surface buoyancy forcing helps to intensify the northward SCSWBC. The Kuroshio Current affects only the northern SCSWBC. It is also concluded that the SCSWC is controlled by the Kuroshio rather than local wind forcing or buoyancy forcing. In winter a part of the SCSWC water comes from the Kuroshio, while in summer the SCSWC water mainly comes from the VCC.

[44] One discrepancy between our model simulations and the observations is the spring basin-scale circulation. *Wyrtki* [1961] shows that the surface current in April is still mostly cyclonic, which is almost identical to that in February except in the southwestern SCS. Our simulations, however, show that the upper ocean circulation in spring has already converted into anticyclonic (Figure 6b). The possible reasons are, first, Figure 6b is for three month averaged and 0–300 m averaged circulation while the observation is for surface layer [*Wyrtki*, 1961]; Second, the model produces deeper thermocline layer and as a result, shorter baroclinic adjustment time for the SCS upper circulation by faster baroclinic Rossby wave; Third, the observation might not be so accurate. This problem needs to be investigated further by more observations and model simulations.

[45] We paid more attention on the SCSWBC system than on the interior circulation because we think the SCSWBC plays much more important roles in the redistribution of the mass, heat, and nutrient than the interior circulation does, especially for the SCS with smaller horizontal scale. Furthermore, the SCSWBC system is much easier to be investigated. It affects more on the human activity and fishery business of the surrounding countries. For examples, the SCSWC usually brings warmer water with high nutrient to the coast off Guangdong Province and may be crucial to the fishery productivity. The variability of VCC reflects the adjustment of the SCS interior circulation, by means of the baroclinic Rossby waves, in response to changing SCS monsoon system. While the SCS monsoon is an indispensable component of the south Asian monsoon system that is strongly related to the planetary-scale atmospheric systems, such as the Walker Circulation and the Cross Equatorial Current coming from Australian High. Therefore studying the variability of SCSWBC provides one clue to understand the interaction of SCS circulation with planetary scale atmospheric circulation on annual, interannual or even decadal timescale. Consequently, more simulations with higher-resolution model are needed to explore the fine structures and dynamics of the SCSWBC.

[46] **Acknowledgments.** We thank E. Bayler for helpful discussions. The altimetry data is downloaded from the Web site of the University of Texas, Center for Space Research. The authors appreciate Roger Ménard at the Marine Environmental Data Service in Canada for providing Argos Buoy data. Comments from two reviewers have helped to improve the manuscript. This work is supported by Natural Science Foundation in China (NSFC) (no.49636230), National Key Program for Developing Basic Science (G1999043807), the NSFC Special program (40028605), DW-XL of Chinese Academy of Sciences (KZCX2-205) and US ONR, NSF, API/UW-Madison (CCR 772).

References

Blumberg, A. F., and G. L. Mellor, A description of a three-dimensional coastal ocean circulation model, in *Three-Dimensional Coastal Ocean Models*, *Coastal Est. Ser.*, vol. 4, edited by N. Heaps, pp. 1–16, AGU, Washington, D. C., 1987.

Cai, S., and J. Su, A two-layer model of the South China Sea (in Chinese), *Acta Oceanogr. Sin.*, *17*(2), 12–20, 1995.

Chambers, D., B. Tapley, and R. Stewart, Long-period ocean heat storage rates and basin-scale heat fluxes from TOPEX, *J. Geophys. Res.*, *102*, 10,525–10,533, 1997.

Chao, S. Y., and P. T. Shaw, El Niño modulation of the South China Sea circulation, *Prog. Oceanogr.*, *38*(1), 51–93, 1996a.

Chao, S. Y., and P. T. Shaw, Deep water ventilation in the South China Sea, *Deep Sea Res. I*, *43*(4), 445–466, 1996b.

Chao, S. Y., P. T. Shaw, and J. Wang, Wind relaxation as a possible cause of the South China Sea Warm Current, *J. Oceanogr.*, *51*, 111–132, 1995.

Chu, P. C., N. L. Edmons, and C. Fan, Dynamical mechanisms for the South China Sea seasonal circulation and thermohaline variabilities, *J. Phys. Oceanogr.*, *29*(11), 2971–2989, 1999.

da Silva, A., C. Young, and S. Levitus, *Atlas of Surface Marine Data 1994*, vol. 1, *Algorithms and Procedures*, NOAA Atlas NESDIS 6, U.S. Dep. of Comm., Washington, D. C., 1994.

Gill, A., and P. Niiler, The theory of the seasonal variability in the ocean, *Deep Sea Res.*, *20*, 141–177, 1973.

Guan, B. X., The South China Sea warm current—A winter counter-wind current in the open sea off the Guang-dong coast (in Chinese), *Oceanol. Limnol. Sin.*, *9*(2), 117–127, 1978.

Guan, B. X., The summer circulation in the Baishi Strait (in Chinese), *J. Oceanogr. Huanghai Bohai Seas*, *8*(4), 1–9, 1990.

Guan, B. X., A review of the South China Sea Warm Current (in Chinese), *Oceanol. Limnol. Sinica*, *29*(3), 322–328, 1998.

Guo, Z. X., T. P. Yang, and D. Z. Qiu, The winter South China Sea warm current and accompanying southwest current (in Chinese), *Tropic Oceanol.*, *4*, 1–9, 1985.

Hellerman, S., and M. Rosenstein, Normal monthly wind stress over the world ocean with error estimates, *J. Phys. Oceanogr.*, *13*, 1093–1104, 1983.

Jerlov, N. G., *Marine Optics*, 231 pp., Elsevier Sci, New York, 1976.

Ho, C. R., Q. Zheng, Y. S. Soong, N. J. Kuo, and J. H. Hu, Seasonal variability of sea surface height in the South China Sea observed with TOPEX/Poseidon altimeter data, *J. Geophys. Res.*, *105*(C6), 13,981–13,990, 2000.

Hu, J., and M. Liu, The current structure of the southern Taiwan Strait in winter and summer (in Chinese), *Trop. Oceanol.*, *11*(4), 42–47, 1992.

Levitus, S., and T. P. Bayer, *World Ocean Atlas*, vol. 3, *Salinity*, U.S. Dep. Comm., Washington, D. C., 1994a.

Levitus, S., and T. P. Bayer, *World Ocean Atlas*, vol. 4, *Temperature*, U.S. Dep. Comm., Washington, D. C., 1994a.

Li, L., and B. Y. Wu, A Kuroshio Loop in the South China Sea? On circulations of the northeastern South China Sea (in Chinese), *J. Oceanogr. Taiwan Strait*, *8*(1), 89–95, 1989.

Li, L., W. D. Nowlin, and J. Su, Anticyclonic rings from the Kuroshio in the South China Sea, *Deep Sea Res., I*, *45*, 1469–1482, 1998.

Li, R., and Q. Zeng, A numerical study of the current systems in the China Sea in winter, *Sci. China Ser. B*, *23*(12), 1329–1338, 1993.

Li, R., Q. Huang, and W. Wang, A simulation of the upper layer current in the South China Sea (in Chinese), *Acta Oceanogr. Sinica*, *16*(4), 13–22, 1994.

Liu, Q. Y., and C. T. Liu, The deformation and dynamic mechanism of the Kuroshio Current in the Luzon Strait (in Chinese), *J. Qingdao Ocean Univ.*, *26*(4), 413–419, 1996.

Liu, X., and J. Su, A reduced model of the South China Sea (in Chinese), *Oceanol. Limnol. Sinica*, *23*(2), 167–174, 1992.

Liu, Z., H. J. Yang, and Q. Y. Liu, Regional dynamics of seasonal variability of sea surface height in the South China Sea, *J. Phys.Oceanogr.*, *31*(1), 272–284, 2001.

Metzger, E. J., and H. E. Hurburt, Coupled dynamics of South China Sea, the Sulu Sea, and the Pacific Ocean, *J. Geophys. Res.*, *111*(C5), 12,331–12,352, 1996.

Pu, S. Z., H. Lin, and S. Nian, The branch of the Kuroshio Current in the Bashi Strait and the northern South China Sea (in Chinese), *Tropic Oceanol.*, *11*(2), 1–7, 1992.

Qiu, D., T. Hong, and Z. Guo, A west flowing current in the northern part of the South China Sea in summer (in Chinese), *Tropic Oceanol.*, *3*(4), 65–73, 1984.

Rong, Z., The analyses of the surface circulation in the South China Sea in winter (in Chinese), *Mar. Forecasts*, *11*(2), 47–51, 1994.

Shaw, P. T., The seasonal variation of the intrusion of the Philippine sea water in the South China Sea, *J. Geophys. Res.*, *96*, 821–827, 1991.

Shaw, P. T., Winter upwelling off Luzon in the Northeastern South China Sea, *J. Geophys. Res.*, *101*(C7), 16,435–16,448, 1996.

Shaw, P. T., and S. Y. Chao, Surface circulation in the South China Sea, *Deep Sea Res., I.*, *41*, 1663–1683, 1994.

Shaw, P. T., S. Y. Chao, and L. Fu, Sea surface height variations in the South China Sea from satellite altimetry, *Oceanol. Acta*, *22*, 1–17, 1999.

Wyrtki, K., Physical oceanography of the Southeast Asia waters, *NAGA Rep.*, *2*, 1–195, 1961.

Xu, X., Z. Qiu, and H. Cheng, A survey of the circulation of the SCS, in *Proceedings of the Chinese Oceanography and Limonology Conference on Hydrological Meteorology* (in Chinese), 137–145, Science Press, Beijing, China, 1980.

Yang, H. J., Simulation of the circulation of the South China Sea (in Chinese), Ph.D. thesis, The Ocean Univ. of Qingdao, Qingdao, China, 2000.

Yang, H. J., and Q. Y. Liu, The seasonal features of temperature distributions in the upper layer of the South China Sea (in Chinese), *Oceanol. Limnol. Sinica*, *29*(5), 501–507, 1999.

X. Liu and D. Wang, South China Sea Institute of Oceanology, Chinese Academy of Sciences, Guangzhou, People's Republic of China.

Z. Liu, Department of Atmospheric and Oceanic Sciences, University of Wisconsin-Madison, Madison, WI 53706, USA.

Q. Liu, Physical Oceanography Laboratory, Ocean University of Qingdao, Qingdao, People's Republic of China.

H. Yang, Department of Atmospheric and Oceanic Sciences, University of Wisconsin-Madison, 1225 West Dayton Street, Madison, WI 53706-1695, USA. (haijunyang@facstaff.wisc.edu)